

Surface Chemistry

Cross-Coupling of Aryl-Bromide and Porphyrin-Bromide on an Au(111) Surface

Guowen Kuang,^[a] Qiushi Zhang,^[a] Deng Yuan Li,^[b] Xue Song Shang,^[b] Tao Lin,^[a] Pei Nian Liu,^{*[b]} and Nian Lin^{*[a]}

Abstract: Cross-coupling is of great importance in organic synthesis. Here it is demonstrated that cross-coupling of aryl-bromide and porphyrin-bromide takes place on a Au(111) surface in vacuo. The products are oligomers consisting of porphyrin moieties linked by *p*-phenylene at porphyrin's *meso*-positions. The ratio of the cross-coupled versus homocoupled bonds can be regulated by the reactant concentrations. Kinetic Monte Carlo simulations were applied to determine the activation barrier. It is expected that this reaction can be employed in other aryl-bromide precursors for designing alternating co-polymers incorporating porphyrin and other functional moieties.

Cross-coupling is a powerful tool available to synthetic chemists in their quest to create new carbon–carbon bonds, while at the same time introducing new carbon- and heteroatom-based functional groups.^[1,2] Cross-coupling reactions allow chemists to design and manipulate delicate and complex molecules.^[3–8] These reactions have been proved useful for the synthesis of many important products, such as drugs, materials, and optical devices.^[9–11] Recently, it has been demonstrated that coupling reactions can take place on solid surfaces, known as on-surface synthesis.^[12–16] In an on-surface reaction, covalent bonds form between molecular precursors that adsorb on a surface; during this process, reactants, intermediates, catalysts and products are confined to a two-dimensional space defined by the surface. Various on-surface reactions, including Ullmann coupling,^[17–22] Glaser coupling,^[23–25] alkane polymerization,^[26] boronic acid condensation,^[27,28] decarboxylative polymerization,^[29] imine coupling,^[30,31] acylation reaction,^[32,33] dimerization of *N*-heterocyclic carbenes,^[34] azide–alkyne cycloadditions,^[35,36] and Bergman cyclizations^[37] have been demonstrated. To a certain extent, on-surface reactions

share fundamental similarities with their counterpart reactions in solution. Nevertheless, on-surface reactions can also follow a significantly different path or mechanism. The special conditions of surface chemistry can be used to synthetic advantage, as on-surface reactions under ultrahigh vacuum (UHV) can be conducted under a much wider range of temperatures than reactions in solution, and two-dimensional confined geometry can invoke reactions not accessible in three dimensions. On-surface synthesis has been used to generate diverse organic systems, including macromolecules,^[18] polymeric chains,^[17,19,26,38] two-dimensional organic networks,^[20,22,24,27,28] and graphene ribbons.^[21]

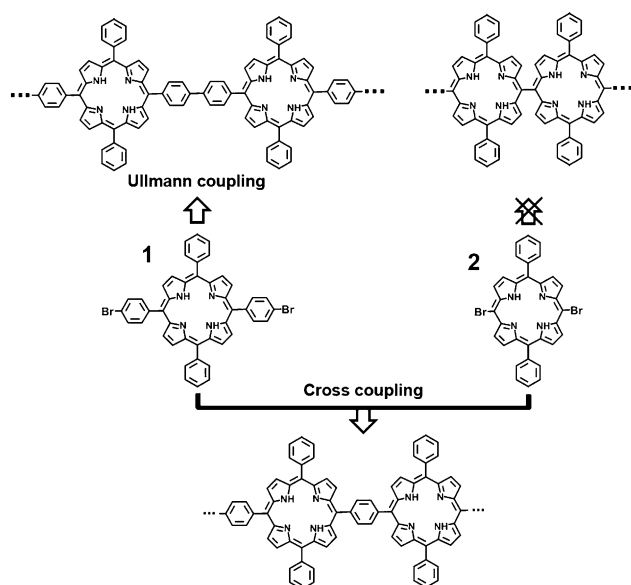
To date, carbon–carbon bond formation by homocoupling reactions has been demonstrated in on-surface synthesis. Cross-coupling reactions, however, have rarely been demonstrated on-surface,^[39] despite their significance in organic synthesis. Here we report on cross-coupling of aryl-bromide (**1**) and porphyrin-bromide (**2**; Scheme 1) on Au(111) surface. This reaction, to our knowledge, has not been reported in organic synthesis. As illustrated in Scheme 1, **1** undergoes homocoupling by Ullmann reaction, but steric hindrance inhibits homocoupling of **2**. Mixing of **1** and **2** generates cross-coupled products of *p*-phenylene-linked porphyrin oligomers. Through analysing the yields of homocoupled and cross-coupled bonds, we quantitatively evaluated the activation barriers of the two coupling reactions, aided by kinetic Monte Carlo simulations. The yield of the cross-coupled bonds could be boosted with excess amount of **2** in the reactant mixture. We found that at a ratio of [2]/[1] = 13 ([2] and [1] stand for molecular dosage of **2** and **1**, respectively, in a unit surface area), 95% of all formed bonds are cross-coupled ones and the products are oligomers with alternating (**12**)_{*n*} morphology.

Homocoupling of molecules of **1** on an Au(111) surface by Ullmann reaction occurs at 180 °C, forming polymeric chains consisting of alternating porphyrin and biphenyl moieties.^[17,40,41] Figure 1a shows a 9-member chain and the inset shows an unreacted monomer. The scanning tunneling microscopy (STM) topograph of the molecules in the chain retains the features of the unreacted monomer, displaying a square-shape morphology with a depression trough in the middle, as marked by the dashed lines in Figure 1a. The molecules thus exhibit twofold symmetry which reflects a nonplanar porphyrin core. This feature corroborates the previous studies reporting the porphyrin core is distorted to a saddle-shape conformation when adsorbed on a metal surface.^[42] Adjacent molecules in the chains are 1.73 nm apart; this is in good agreement with

[a] G. Kuang, Q. Zhang, Dr. T. Lin, Prof. Dr. N. Lin
Department of Physics
The Hong Kong University of Science and Technology
Clear Water Bay (Hong Kong)
E-mail: phnlin@ust.hk

[b] D. Y. Li, X. S. Shang, Prof. Dr. D. N. Liu
Shanghai Key Laboratory of Functional Materials Chemistry and
Institute of Fine Chemicals, East China University of Science and
Technology, Meilong Road 130, Shanghai (P. R. China)
E-mail: liupn@ecust.edu.cn

Supporting information for this article is available on the WWW under
<http://dx.doi.org/10.1002/chem.201501095>.



Scheme 1. Cross-coupling of aryl-bromide (1) and porphyrin-bromide (2). Homocoupling of porphyrin-bromide is inhibited by steric hindrance.

the structural model shown in Figure 1b. Note that the 9-member chain is not perfectly straight: the chain bends 26° wherever the troughs of two neighbouring molecules are not parallel. We propose that this non-straight morphology is associated with the distorted porphyrin core. The model in Figure 1b highlights the saddle-shaped conformation: two up-titled pyrrole moieties are shaded and the troughs are represented by the dashed lines. It has been reported that four phenyl moieties at the *meso*-positions of a saddle-shaped porphyrin core point to different orientations.^[42] Accordingly, the two opposite phenyl moieties in a molecule are not co-linear, as drawn schematically in the model. With such a molecular conformation, the chain is bent where two adjacent molecules have differently orientated troughs, as illustrated in Figure 1b.

Molecules of **2** self-assemble as closely packed molecular islands on Au(111) as prepared at room temperature and after 180°C annealing, as shown in Figure 2a and b, respectively. The inset in Figure 2b features a single molecule, displaying a depressed central region and two protruding ends that can be assigned to two phenyl moieties. A structural model is overlaid on the STM topograph. Presumably, the porphyrin core is closer to the substrate, whereas the phenyl moieties rotate out of the molecular plane with a large dihedral angle, giving rise to the bright ends. We use dotted ellipses to mark out single molecules in the closely packed molecular islands in Figure 2a and b. Close inspection of Figure 2a and b reveals that the molecules arrange differently before and after 180°C annealing. Each molecule occupies 1.48 nm^2 (1.35 nm^2) before (after) the annealing. So the molecules are packed slightly denser after the annealing. The structural change hints that the annealing has altered intermolecular interactions. We speculate this change is associated with debromination of **2**, which has taken place at 180°C annealing. The molecular models of the two closely packed islands are drawn in Figure 2a and b, re-

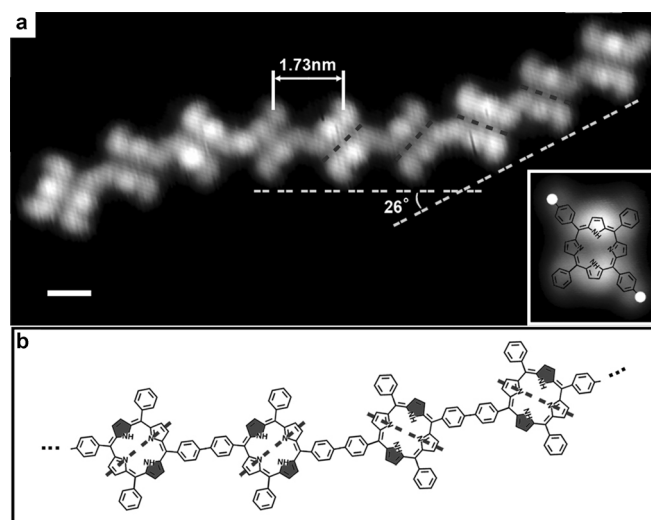


Figure 1. a) STM topograph of a polymeric chain formed by Ullmann coupling of **1**. The scale bar is 1 nm. Inset ($2.24 \times 2.58\text{ nm}^2$): an unreacted monomer of **1** with the structural model overlaid (the bromine ends are highlighted by dots). b) Structural model of the polymeric chain illustrating the saddle-shaped porphyrin core and the bending morphology.

spectively. In an attempt to use catalysts to promote homocoupling of **2**, we deposited Cu and **2** on Au(111). After annealing at 200°C , chain-like structures formed. The chains comprise an organometallic compound in which neighbouring porphyrin molecules are linked by C–Cu–C bonds (see the detailed description in the Supporting Information). Apparently, unlike **1**, **2** does not undergo homocoupling even when the bromine atoms cleaved off. We further annealed this sample at up to 250°C , and observed that the molecules still formed islands of the same structure shown in Figure 2b, but not any covalently linked chain-like structures. So we conclude that homocoupling of **2** does not occur on Au(111) surface up to 250°C with or without Cu deposition.

Considering that Cu surface is more reactive than Au in activating on-surface Ullmann coupling,^[43–45] we deposited **2** on a Cu(111) surface held at room temperature. Figure 2c shows that the molecules organize as linear chain-like structures. The adjacent molecules in a chain are spaced at 1.20 nm. This distance agrees well with an organometallic compound in which neighbouring porphyrin moieties are linked by C–Cu–C bonds,^[38] as illustrated by the model in Figure 2d, with a C–Cu distance of 2.5 \AA . Because formation of the organometallic compounds associates with debromination, debromination of **2** must take place at room temperature on Cu(111). As discussed above, the same reaction is activated by 180°C annealing on Au(111). This contrast indicates that the Cu surface catalyses debromination of **2**. Annealing this sample at 200°C dissolved the organometallic structures, however, did not result in covalently linked structures. Instead, individual molecules are scattered on the surface (Figure 2e). We speculate that the molecules of **2** undergo conformational distortion at high temperature and consequently bind the substrate Cu atoms strongly. This molecule–substrate bonding prevents the molecules from forming the organometallic chains or the ordered

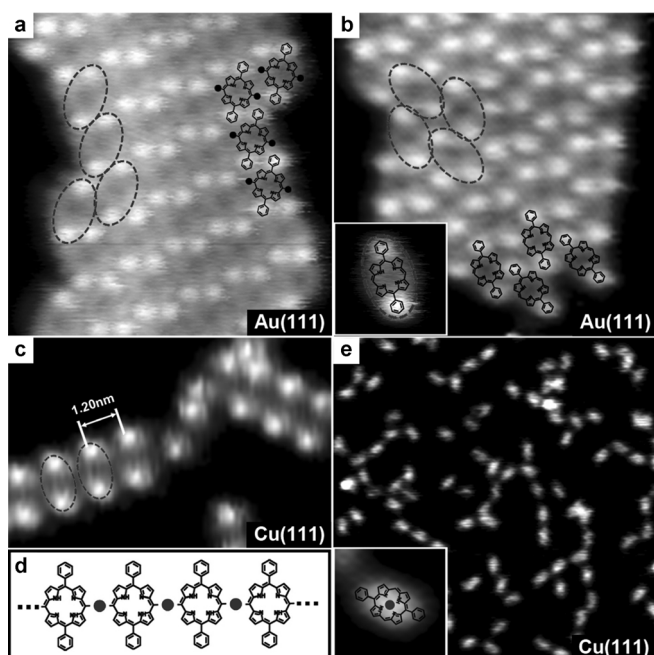


Figure 2. STM topographs ($8 \times 8 \text{ nm}^2$) showing closely packed molecular islands assembled by **2** on Au(111): a) at room temperature, and b) after annealing at 180°C . Inset (b; $2.5 \times 2.5 \text{ nm}^2$): a single molecule with a structural model overlaid. Dotted ellipses mark out single molecules. c) Organometallic chains formed by **2** at room temperature on Cu(111) ($10 \times 6.5 \text{ nm}^2$). d) Structural model of the organometallic chains (dots represent Cu atoms). e) Molecules of **2** scattered on Cu(111) after annealing at 200°C ($30 \times 30 \text{ nm}^2$). Inset ($2.5 \times 2.5 \text{ nm}^2$): a single molecule with a model overlaid showing metalation of the porphyrin core.

molecular islands. Note that the molecules now appear brighter at the centre (Figure 2e, inset), presumably due to metalation of the porphyrin core by Cu atoms,^[46–48] as illustrated by the overlaid molecular model in Figure 2e (inset). In conclusion, homocoupling of **2** does not take place on Cu(111) surface either. We attribute this behaviour to steric hindrance. It has been reported that derivatives of **2** can be covalently linked as oligomers in solution phase.^[49–51] In these oligomers, the neighbouring porphyrin moieties do not align in co-planar conformation, but have a nearly 90° dihedral angle. As confined on a surface, however, the porphyrin cores are parallel to the surface. Supposing that two co-planar porphyrin cores are linked by a C–C bond at their *meso*-position, the hydrogen atoms at the beta-positions will overlap in space. We propose that steric repulsion inherently hinders on-surface homocoupling of **2**.

To achieve cross-coupling of **1** and **2**, both species were deposited on the Au(111) surface at room temperature, after which the sample was annealed at 180°C . STM (Figure 3a) reveals closely packed ribbon-shaped islands composed of molecules of **2** (see detailed description in the Supporting Information) as pointed by the arrow, and many oligomer structures. An example of these oligomers is shown in Figure 3b. One can see that the oligomer consists of wide and narrow motifs, denoted as motif-1 and motif-2, respectively, hereafter. Motif-1 has a shape resembling **1** (Figure 1a) whereas motif-2 resembles **2** (Figure 2b). We found that the motif-2 species are

always connected with those of motif-1, whereas the motif-1 species can be connected with both types. The distance between two adjacent motif-1 species is 1.73 nm , while the distance between a motif-1 and a motif-2 species is 1.30 nm . Based on the spacing and their characteristic shapes, we assign the motif-1 species to **1**, and the motif-2 species to **2**. The oligomer shown in Figure 3b is thus a chain of **1112** sequence. In the same way, we are able to unambiguously determine the sequence of any oligomers. Figure 3c shows some examples of the oligomers featuring **2112**, **12**, **112**, and **211112** sequences. Apparently, both homocoupling of **1** and cross-coupling between **1** and **2** happened in the on-surface reactions.

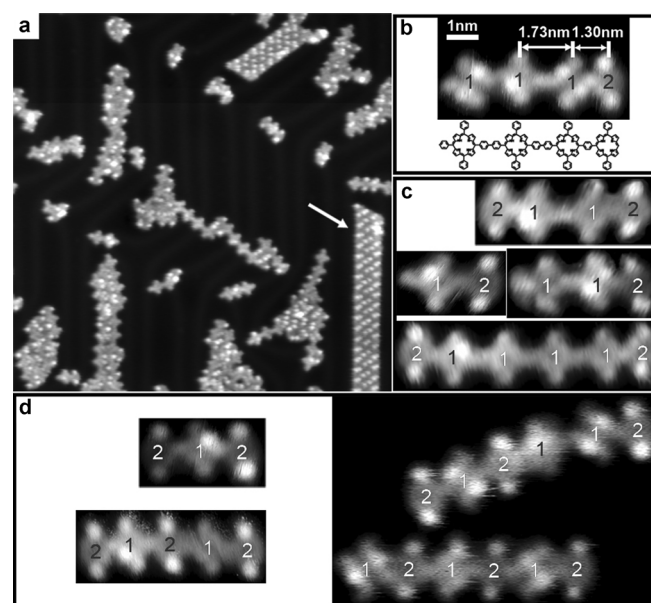


Figure 3. a) STM topograph ($50 \times 50 \text{ nm}^2$) showing the oligomers formed out of a mixture of **1** and **2**. b) A magnified STM topograph of a **1112** oligomer with a structural model. c) Selected oligomers formed in sample 1 with their sequences marked. d) Selected oligomers formed in sample 3 exhibiting alternating sequences. The images in c) and d) are in the same scale as b).

We conducted statistical analysis to quantify the yields of the homocoupling and cross-coupling reactions (Table 1). In sample 1, at the concentration ratio of the two molecules $[\mathbf{2}]/[\mathbf{1}] = 1.6$, 85% of molecules **1** and 29% of molecules **2** are coupled. Among the formed bonds, 40% are homocoupled and 60% are cross-coupled. We tested how reactant concentration may affect the yields of homo- and cross-coupling. In sample 2, the molecule dosage was increased 2.5-fold while the ratio of $[\mathbf{2}]/[\mathbf{1}]$ remained at 1.6. After the same annealing process as conducted on sample 1, 75% of molecules **1** and 24% of molecules **2** are coupled; 36% of the bonds formed are the result of homocoupling and 64% the result of cross-coupling (Table 1). To conclude, varying the concentration but not the ratio of the two reactants does not alter the yield of the cross-coupling significantly. To boost the cross-coupling yield, we raised the ratio $[\mathbf{2}]/[\mathbf{1}]$ to 13 in sample 3, while maintaining the total molecule concentration as in sample 1. We found that

95% of the coupled bonds are the result of cross-coupling (Table 1), indicating that cross-coupling predominates over homocoupling. Some examples of the oligomers formed in sample 3 are shown in Figure 3d, exhibiting **212**, **21212**, **212112** and **121212** sequences. These examples demonstrate that the cross-coupling may generate oligomers with alternating morphology at this unbalanced reactant concentration. The drawback of this protocol is that a large amount (~90%) of molecules of **2** are not used.

Table 1. Statistical analysis of homocoupled and cross-coupled bonds that formed in three samples with different reactant concentrations.^[a]

	Sample 1	Sample 2	Sample 3
[1] per 100 nm ²	4.6	11	0.8
[2] per 100 nm ²	7.5	18	10
[2]/[1]	1.6	1.6	13
[coupled 1]/[1]	85%	75%	95%
[coupled 2]/[2]	29%	24%	11%
[homocoupled]	40%	36%	5%
[cross-coupled]	60%	64%	95%

[a] Molecules counted: 2656 (**1**) and 4320 (**2**) in sample 1, 1357 (**1**) and 2209 (**2**) in sample 2, and 1612 (**1**) and 21278 (**2**) in sample 3.

Furthermore, we analysed the length of the alternating chains formed in the three samples and obtained chain-length distributions. Polymerization is generally categorized as step-growth, which results in a monotonous decay length distribution, or chain-growth, which results in a Poisson-type length distribution.^[52] As shown in Figure 4a, the chains formed in sample 1 and 2 ([2]/[1]=1.6) exhibit a monotonous decay chain-length distribution, suggesting that the cross-coupling reaction leads to a typical step-growth polymerization. The average chain length is 2.75 monomers. Interestingly, the chain-length distribution of sample 3 ([2]/[1]=13) deviates from a monotonous decay, showing that the odd-numbered chains become more abundant as compared with the shorter even-numbered ones. Presumably, this is due to the effect that excessive amount of molecules **2** terminate both ends of the chains, thus resulting in odd-numbered chains. The average chain length in this sample is slightly longer, 2.94 monomers.

We performed kinetic Monte Carlo (kMC) simulations to evaluate the activation barriers, E_H and E_C , of the homocoupling and the cross-coupling reactions, respectively. The details of the kMC simulation algorithm can be found in the Supporting Information. In the simulations, the total concentration of the two species, [1] + [2], was set in accordance with the experimental samples 1 and 3. Figure 4c shows the simulated structures formed with [2]/[1]=1.6. The crosses with dark and grey bars represent molecules of **1** and **2**, respectively. The white tips represent bromine ends, and the black bars the C–C bonds formed in the coupling reaction. We found that by setting $E_H=1.20$ eV^[41] and $E_C=1.24$ eV, the outcome of the simulations is in good agreement with the experimental results, including the percentages of **1** and **2** molecules that are coupled, the yields of homocoupled and cross-coupled bonds. The

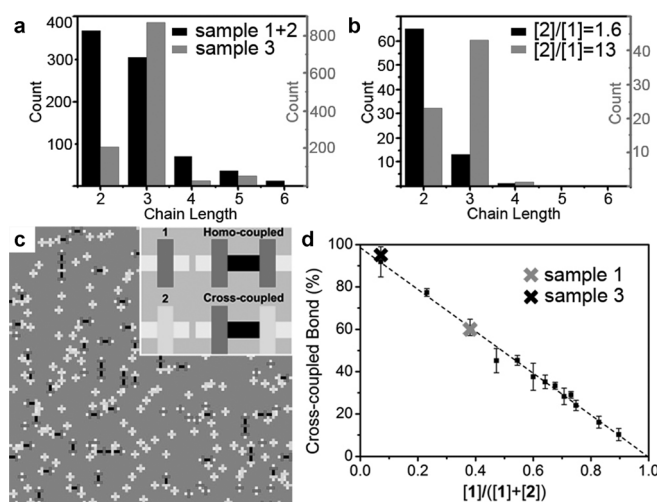


Figure 4. a) Chain-length distribution histogram of sample 1 and 3. b) kMC simulated chain-length distribution. c) kMC simulated structures with [2]/[1]=1.6. The crosses containing dark and grey bars represent **1** and **2**, respectively, the white tips stand for the bromine ends. The black bars indicate the C–C bonds formed in the coupling reaction. d) Yield of cross-coupled bonds as a function of [1]/([1] + [2]).

simulated yields of the cross-coupled bond as a function of [1]/([1] + [2]) are plotted in Figure 4d (the crosses mark the experimental values in samples 1 and 3, respectively). The linear decay trend shows that the concentration of **1** in the reactant mixture regulates the yield of the cross-coupled bonds. Moreover, the chain-length distributions of the simulated chains at the two experimental conditions (Figure 4b) reproduce the experimental data.

In summary, we have demonstrated that cross-coupling of aryl-bromide and porphyrin-bromide can be achieved on a Au(111) surface. The products are oligomers of porphyrin linked by *p*-phenylene moiety at *meso*-positions. The detailed mechanism of this reaction is subject for further study. We expect that this reaction can be employed in other aryl-bromide precursor molecules for designing alternating co-polymers incorporating porphyrin and other functional moieties.

Experimental Section

Experiments were performed in an ultrahigh-vacuum system (Omicron Nanotechnology) with base pressure below 5×10^{-10} mbar. A single-crystalline Au(111) substrate was cleaned by Argon-ion sputtering and annealing to approximately 630 °C. Molecules **1** and **2** were thermally evaporated by a molecular beam evaporator and deposited onto the Au(111) substrate which was held at room temperature. The evaporation temperatures for molecules **1** and **2** were 325 and 285 °C, respectively. The STM images were acquired at 77 K and the STM imaging parameters were $U=-1.00$ V, $I=0.30$ nA.

The kinetic Monte Carlo (kMC) simulations were performed on a 100×100 square lattice. Periodic boundary condition was applied. Molecule **1** and **2** take a cross shape with two opposite tips as Br atoms. Each molecule occupies 3×3 sites, so, 33×33 molecules fully cover the substrate lattice sites. Molecule **1** and **2** with defined ratio are deposited randomly onto the substrate lattice.

Desorption of the molecule from the substrate was not allowed. The molecules can hop to the nearest-neighbouring site or rotate by 90° clockwise or anti-clockwise. The rates of each event are given by $r = v \times \exp(-E/kT)$, where v is the prefactor and k Boltzmann constant. The prefactor is set as 1×10^{12} Hz. The energy barriers of diffusion and rotation for both molecules are set 0.74 and 1.00 eV, respectively.^[2] When one molecule encounters another molecule in a Br–Br configuration, a rate for the formation of a covalent bond is generated as determined by an activation barrier. The activation barriers for homocoupling of **1** is set as 1.20 eV,^[3] homocoupling of **2** as 10.00 eV and cross-coupling of **1+2** as 1.24 eV.

Acknowledgements

This work was supported financially by the Hong Kong Research Grants Council (project no. 603213), the National Natural Science Foundation of China (project nos. 21172069, 21190033 and 21372072) and the Science Fund for Creative Research Groups (21421004).

Keywords: cross-coupling · gold · kinetic Monte Carlo simulation · scanning tunneling microscopy · surface chemistry

- [1] F. Diederich, P. J. Stang, *Metal-Catalyzed Cross-coupling Reactions*, Wiley-VCH, Weinheim, 1998.
- [2] A. de Meijere, F. Diederich, *Metal-Catalyzed Cross-Coupling Reactions*, Wiley-VCH, Weinheim, 2nd ed., 2004, Vols. 1 and 2.
- [3] J.-P. Corbet, G. R. Mignani, *Chem. Rev.* **2006**, *106*, 2651–2710.
- [4] A. Fihri, M. Bouhrara, B. Nekoueshahraki, J.-M. Bassat, V. Polshettiwar, *Chem. Soc. Rev.* **2011**, *40*, 5181–5203.
- [5] G. C. Fortman, S. P. Nolan, *Chem. Soc. Rev.* **2011**, *40*, 5151–5169.
- [6] J. D. Sellars, P. G. Steel, *Chem. Soc. Rev.* **2011**, *40*, 5170–5180.
- [7] Y. Nakao, T. Hiyama, *Chem. Soc. Rev.* **2011**, *40*, 4893–4901.
- [8] S. Z. Tasker, E. A. Standley, T. F. Jamison, *Nature* **2014**, *509*, 299–309.
- [9] E. Negishi, *Angew. Chem. Int. Ed.* **2011**, *50*, 6738–6764; *Angew. Chem.* **2011**, *123*, 6870–6897.
- [10] K. C. Nicolaou, P. G. Bulger, D. Sarlah, *Angew. Chem. Int. Ed.* **2005**, *44*, 4442–4489; *Angew. Chem.* **2005**, *117*, 4516–4563.
- [11] J. Magano, J. R. Dunetz, *Chem. Rev.* **2011**, *111*, 2177–2250.
- [12] J. A. A. W. Elemans, S. B. Lei, S. De Feyter, *Angew. Chem. Int. Ed.* **2009**, *48*, 7298–7332; *Angew. Chem.* **2009**, *121*, 7434–7469.
- [13] M. Lackinger, W. M. Heckl, *J. Phys. D* **2011**, *44*, 464011.
- [14] D. F. Perepichka, F. Rosei, *Science* **2009**, *323*, 216–217.
- [15] A. Gourdon, *Angew. Chem. Int. Ed.* **2008**, *47*, 6950–6953; *Angew. Chem.* **2008**, *120*, 7056–7059.
- [16] J. Méndez, M. F. Lopez, J. A. Martin-Gago, *Chem. Soc. Rev.* **2011**, *40*, 4578–4590.
- [17] L. Grill, M. Dyer, L. Lafferentz, M. Persson, M. V. Peters, S. Hecht, *Nat. Nanotechnol.* **2007**, *2*, 687–691.
- [18] Q. T. Fan, C. Wang, Y. Han, J. Zhu, W. Hieringer, J. Kuttner, G. Hilt, J. M. Gottfried, *Angew. Chem. Int. Ed.* **2013**, *52*, 4668–4672; *Angew. Chem.* **2013**, *125*, 4766–4770.
- [19] J. A. Lipton-Duffin, O. Ivashenko, D. F. Perepichka, F. Rosei, *Small* **2009**, *5*, 592–597.
- [20] R. Gutzler, H. Walchm, G. Eder, S. Kloft, W. M. Heckl, M. Lackinger, *Chem. Commun.* **2009**, 4456–4458.
- [21] J. M. Cai, P. Ruffieux, R. Jaafar, M. Bieri, T. Braun, S. Blankenburg, M. Muoth, A. P. Seitsonen, M. Saleh, X. L. Feng, K. Mullen, R. Fasel, *Nature* **2010**, *466*, 470–473.
- [22] L. Lafferentz, V. Eberhardt, C. Dri, C. Africh, G. Comelli, F. Esch, S. Hecht, L. Grill, *Nat. Chem.* **2012**, *4*, 215–220.
- [23] H. Y. Gao, H. Wagner, D. Zhong, J. H. Franke, A. Studer, H. Fuchs, *Angew. Chem. Int. Ed.* **2013**, *52*, 4024–4028; *Angew. Chem.* **2013**, *125*, 4116–4120.
- [24] Y. Q. Zhang, N. Kepčija, M. Kleinschrodt, K. Diller, S. Fischer, A. C. Papa-georgiou, F. Allegretti, J. Björk, S. Klyatskaya, F. Klappenberger, M. Ruben, J. V. Barth, *Nat. Commun.* **2012**, *3*, 1286.
- [25] H. T. Zhou, J. Z. Liu, S. X. Du, L. Z. Zhang, G. Li, Y. Zhang, B. Z. Tang, H. J. Gao, *J. Am. Chem. Soc.* **2014**, *136*, 5567–5570.
- [26] D. Y. Zhong, J. H. Franke, S. K. Podiyanchari, T. Blomker, H. M. Zhang, G. Kehr, G. Erker, H. Fuchs, L. F. Chi, *Science* **2011**, *334*, 213–216.
- [27] N. A. A. Zwaneveld, R. Pawlak, M. Abel, D. Catalin, D. Gigmes, D. Bertin, L. Porte, *J. Am. Chem. Soc.* **2008**, *130*, 6678–6679.
- [28] J. F. Dienstmaier, D. D. Medina, M. Dogru, P. Knochel, T. Bein, W. M. Heckl, M. Lackinger, *ACS Nano* **2012**, *6*, 7234–7242.
- [29] H. Y. Gao, P. A. Held, M. Knor, C. Muck-Lichtenfeld, J. Neugebauer, A. Studer, H. Fuchs, *J. Am. Chem. Soc.* **2014**, *136*, 9658–9663.
- [30] S. Weigelt, C. Busse, C. Bombis, M. M. Knudsen, K. V. Gothelf, T. Strunskus, Ch. Woll, M. Dahlbom, B. Hammer, E. Laegsgaard, F. Besenbacher, T. R. Linderoth, *Angew. Chem. Int. Ed.* **2007**, *46*, 9227–9230; *Angew. Chem.* **2007**, *119*, 9387–9390.
- [31] S. Weigelt, C. Busse, C. Bombis, M. M. Knudsen, K. V. Gothelf, E. Laegsgaard, F. Besenbacher, T. R. Linderoth, *Angew. Chem. Int. Ed.* **2008**, *47*, 4406–4410; *Angew. Chem.* **2008**, *120*, 4478–4482.
- [32] M. Treier, N. V. Richardson, R. Fasel, *J. Am. Chem. Soc.* **2008**, *130*, 14054–14055.
- [33] A. C. Marele, R. Mas-Balleste, L. Terracciano, J. Rodriguez-Fernandez, I. Berlanga, S. S. Alexandre, R. Otero, J. M. Gallego, F. Zamora, J. M. Gomez-Rodriguez, *Chem. Commun.* **2012**, *48*, 6779–6781.
- [34] M. Matena, T. Riehm, M. Stöhr, T. A. Jung, L. H. Gade, *Angew. Chem. Int. Ed.* **2008**, *47*, 2414–2417; *Angew. Chem.* **2008**, *120*, 2448–2451.
- [35] F. Bebensee, C. Bombis, S. R. Vadapoo, J. R. Cramer, F. Besenbacher, K. V. Gothelf, T. R. Linderoth, *J. Am. Chem. Soc.* **2013**, *135*, 2136–2139.
- [36] O. Díaz Arado, H. Monig, H. Wagner, J. H. Franke, G. Langewisch, P. A. Held, A. Studer, H. Fuchs, *ACS Nano* **2013**, *7*, 8509–8515.
- [37] Q. Sun, C. Zhang, Z. W. Li, H. H. Kong, Q. G. Tan, A. G. Hu, W. Xu, *J. Am. Chem. Soc.* **2013**, *135*, 8448–8451.
- [38] W. H. Wang, X. Q. Shi, S. Y. Wang, M. A. Van Hove, N. Lin, *J. Am. Chem. Soc.* **2011**, *133*, 13264–13267.
- [39] C. Sanchez-Sanchez, N. Orozco, J. P. Holgado, S. K. Beaumont, G. Kyriakou, D. J. Watson, A. R. Gonzalez-Elipe, L. Ferial, J. F. Sanz, R. M. Lambert, *J. Am. Chem. Soc.* **2015**, *137*, 940–947.
- [40] T. Lin, X. S. Shang, J. Adisojoso, P. N. Liu, N. Lin, *J. Am. Chem. Soc.* **2013**, *135*, 3576–3582.
- [41] J. Adisojoso, T. Lin, X. S. Shang, K. J. Shi, A. Gupta, P. N. Liu, N. Lin, *Chem. Eur. J.* **2014**, *20*, 4111–4116.
- [42] A. Weber-Bargioni, W. Auwärter, F. Klappenberger, J. Reichert, S. Lefrançois, T. Strunskus, Ch. Wöll, A. Schiffrin, Y. Pennec, J. V. Barth, *ChemPhysChem* **2008**, *9*, 89–94.
- [43] M. T. Nguyen, C. A. Pignedoli, D. Passerone, *Phys. Chem. Chem. Phys.* **2011**, *13*, 154–160.
- [44] J. Björk, F. Hanke, S. Stafström, *J. Am. Chem. Soc.* **2013**, *135*, 5768–5775.
- [45] M. Bieri, M. T. Nguyen, O. Gröning, J. Caim, M. Treier, K. Ait-Mansour, P. Ruffieux, C. A. Pignedoli, D. Passerone, M. Kastler, K. Müllen, R. Fasel, *J. Am. Chem. Soc.* **2010**, *132*, 16669–16676.
- [46] K. Diller, F. Klappenberger, M. Marschall, K. Hermann, A. Nefedov, Ch. Wöll, J. V. Barth, *J. Chem. Phys.* **2012**, *136*, 014705.
- [47] S. Ditzel, M. Stark, M. Drost, F. Buchner, H.-P. Steinrueck, H. Marbach, *Angew. Chem. Int. Ed.* **2012**, *51*, 10898–10901; *Angew. Chem.* **2012**, *124*, 11056–11059.
- [48] M. Stark, S. Ditzel, M. Lepper, L. Zhang, H. Schlott, F. Buchner, M. Rockert, M. Chen, O. Lytken, H.-P. Steinrueck, H. Marbach, *Chem. Commun.* **2014**, *50*, 10225–10228.
- [49] N. Aratani, A. Osuka, Y. H. Kim, D. H. Jeong, D. Kim, *Angew. Chem. Int. Ed.* **2000**, *39*, 1458–1462; *Angew. Chem.* **2000**, *112*, 1517–1521.
- [50] A. Tsuda, A. Osuka, *Science* **2001**, *293*, 79–82.
- [51] N. Aratani, A. Takagi, Y. Yanagawa, T. Matsumoto, T. Kawai, Z. S. Yoon, D. Kim, A. Osuka, *Chem. Eur. J.* **2005**, *11*, 3389–3404.
- [52] P. J. Flory, *Principles of Polymer Chemistry*, Cornell University Press, Ithaca, 1953.

Received: March 20, 2015
Published online on April 16, 2015